UNIVERSITY "POLITEHNICA" OF BUCUREŞTI
FACULTY OF ELECTRONICS
TELECOMMUNICATION AND INFORMATION
TECHNOLOGY

Non-linear image representation and pixel-wise processing for enhancing images acquired with digital cameras

Corneliu FLOREA

PhD Supervisor: prof. Vasile BUZULOIU

Contents

Chapter 1

Introduction

This work focuses on processing of images captured with digital still camera. Why digital still cameras? Because nowadays these are, arguably, the most used, common and cheap mean of acquiring digital images; and images are the most important way of communication between people. Digital still camera, as well as human eye, is a non-linear image device. Therefore, a dedicated algorithm must imply non-linear techniques. To address this problems, two methods are at hand: one relies on using non-linear operators[1] and the other intercalates non-linear transformations with linear operators.

In this work we shall focus on developing non-linear operators. The starting point lies in the homomorphic theory introduced by Oppenheim, [1] and in logarithmic image processing models proposed, by Jourlin–Pinoli and Pătraşcu and lately by Vertan. These are the known solutions and the arising question if these are the only ones? A mathematical investigation that set the boundaries for such models, an analysis of the existing ones and means for deriving new models is the goal of the chapter 2. This part is a more theoretical one and provides the background for the following practical applications.

The second part of the current work details two practical applications that enhance images acquired with digital still camera. But before describing the actual methods, there is need for a short presentation of the constructive characteristics of cameras, so to be able to adapt the method to the given device. The overview of the camera model and of the implicit image processing algorithms will be provided in chapter 3.

[1] In the current paper we shall describe non-linear models of image representation. These models are non-linear in respect to the widely used real intensity based models. The operators (addition and scalar multiplication) derived within the new structures are linear in respect to their parent model. However if the reference are the operators from the classical real numbers space, the new operators are non-linear. For simplicity of formulation, we shall name them "non-linear operators".

Once the theoretical background and the particular feature of the input device are known, the processing method will be in focus. In fact two applications are addressed. One regards digital still cameras' most important problem. That is image degradation due to motion blur when high exposure time meets hand-held devices. The proposed solution, as presented in chapter 4, uses a shorter exposure time for the acquisition of the subject image to reduce the motion blur and, consequently, amplifies the recorded images by using information from a second (namely a reference one) picture of the same scene.

The second application, described in chapter 5, refers to dynamic range enhancement of the images acquired with digital still camera. The current approach uses the non-linearity of logarithmic image processing models to push further the results of the typical bracketing solution. The classical bracketing algorithm combines several differently exposed frames to reconstruct the high value of the gamut of the scene. In the current work, we shall prove that adding weights to the input frames and non-linear image fusion, boost the resulting dynamic range, leading, in fact, to an over-sampling of the output space. We named this algorithm "log–bracketing". Even if the algorithm addresses color images, perhaps one of its most important application will be in digitizing analog radiographs. The most simple solution for the mentioned digitization is to photograph the analog X-ray film; however this choice has the drawback of decreasing the dynamic range from 2^{12} levels (36 dB), in the original analog image, to 8 bits (24 dB) in the resulting digital one. The loss of information may be counterweighted by the use of presented algorithm.

The last chapter will summarize the achievements and will conclude the current work. It will also provide a look to further continuations.

Chapter 2

Non-linear Image Processing Models

The Logarithmic Image Processing (LIP) Models represent an alternative to image processing with real based operations. Under certain circumstances, such a combination, named Classical Linear Image Processing (CLIP) - [2] proves its limitations. For instance, let us mention the upper range overflow, which is brutally solved by truncation. Consequently, more elaborate structures appeared, such as the LIP models: Jourlin–Pinoli model, [3], and Pătraşcu model [4]. Recently a new model, which turns aside from the logarithmic form, has been proposed by Vertan et.al, [5]. In such a context, the "logarithm" syntagma should be replaced with the more general "non–linear" one.

The non-linear image processing (NIP) models proved their usefulness in various applications like illumination correction, [6], contrast enhancement, [7], [8], edge detection, [5], dynamic range enhancement, [8], [9], [10]. The improve in respect to the classical methods has been proven. Yet we believe that the best results have not been achieved. Further advance is reachable by extension of the existing NIP models.

Before detailing the actual expanding technique, we investigate the theoretical boundaries of a NIP model. Once we shall identify these limits, we shall propose various methods to extend the current model by either constructing new models, or by parametrization.

2.1 Mathematical Background of Non-Linear Image Processing Models

The mathematical construction of such a non-linear model may start by defining the operational laws (the addition and the scalar multiplication) or, equivalently, by finding the function that maps the investigated model definition set onto the real number algebraic

structure and, hence, acts as a generative mapping. We will focus on the second alternative and we will investigate the restrictions that have to be imposed to the mapping (generative function), such that the new model will lead to a consistent mathematical form and, thus, will exhibit practical properties. Usually the model forms a vector space or a cone structure, [11], [12]. In this section we shall investigate the nature of the definition set, the means of laws determination, the closing properties and we shall discuss the requirements needed to form a vector space. The hereby mathematical formulation is a particular case of the more general homomorphic theory, applied to discrete images.

2.1.1 Vector/Cone Space Structure

Let us consider a function, $\Phi : E \rightarrow F$. Within this choice, the set E is the image definition set. Typically, if the image values have intensity meaning, the set is bounded.

The function Φ defines the model structure and maps the image definition set, E, onto a subset of real numbers, F. Furthermore, we shall add two operations to the given set, E: addition of two elements of the set, $\oplus$, and multiplication with an outer scalar, $\otimes$. Given a real scalar, $\alpha \in K \subseteq \mathbb{R}$, and two elements of the set, u and v, we can determine the exact formulas for the mentioned operations using the generative function Φ:

$$\Phi(u \oplus v) = \Phi(u) + \Phi(v) \tag{2.1}$$

$$\Phi(\alpha \otimes u) = \alpha\Phi(u) \tag{2.2}$$

Equations (2.1) and (2.2) are the conditions that must be fulfilled by a homomorphism between two similar algebraic structures. In our approach, we assume the function Φ to be known and we intend to use the mentioned relations to determine the analytic form of the addition and scalar multiplication laws. In such a case, the simplest solution is achieved when the function is a bijection and, hence, the laws are uniquely determined.

With respect to the bijectivity constraint (and, hence, the existence of Φ^{-1}), the definition laws are determined by:

$$u \oplus v = \Phi^{-1}\left(\Phi(u) + \Phi(v)\right) \tag{2.3}$$

$$\alpha \otimes u = \Phi^{-1}\left(\alpha\Phi(u)\right) \tag{2.4}$$

A short analysis of equation (2.1) and (2.2) written for the boundary points of the definition set E will lead to an infinite width of the target set $F : [0; +\infty)$.

An important feature of the NIP models is the closing property of both addition and scalar multiplication. This states that the sum of any two images should lead to another valid image and, respectively, any amplified or attenuated image should be an image:

$$\begin{aligned} \forall u, v \in E \quad z = u \oplus v \Rightarrow z \in E \\ \forall u \in E, \forall \alpha \in K \quad z = \alpha \otimes u \Rightarrow z \in E \end{aligned} \tag{2.5}$$

These properties hold under the assumed bijectivity hypothesis.

Given the two operative laws, $\oplus$, $\otimes$, the vector set E and the outer scalar set K, the formal definition of the vector space implies several properties. The addition law must be associative, commutative, must have identity element and inverse element. The distributivity must hold for scalar multiplication over vector addition and for scalar multiplication in the field of scalars. Scalar multiplication must have identity element and must be compatible with multiplication in the field of scalars.

The commutative, associative and distributive properties of the implied laws are important because the order of operations should not matter in a weighted sum of images. Under the assumed hypothesis of bijective application, these properties are verified.

The existence of the identity element, u_0, with respect to the addition, implies further condition over the mapping function, Φ. The mentioned restriction is a consequence of the isomorphic behavior:

$$\forall u \in E, \;\; \exists u_0, \;\; u \oplus u_0 = u \Leftrightarrow \Phi(u_0) = 0 \tag{2.6}$$

The existence of addition inverse element, u^- is conditioned by a symmetry towards 0 of the generative function. It makes the difference between vector and cone space. However, since this is not of paramount importance for the physical interpretation of such a model, it is not un–common to avoid it. The consequence is that, in many cases the NIP model has a cone structure.

Similarly with addition, the identity element of the scalar multiplication has to be 1:

$$\exists \alpha_1, \forall u \in E - \{u_0\}, \;\; \alpha_1 \otimes u = u \Leftrightarrow \alpha_1 = 1 \tag{2.7}$$

In conclusion, the sufficient conditions that a generative function, Φ, has to fulfill in order to generate a usable non-linear image processing model are:

- The target F should be at least $[0; \infty)$ in the case of cone structure;
- Φ should be bijective;
- $\Phi(u_0) = 0$.

2.2 Non-linear Image Processing Models

2.2.1 Jourlin – Pinoli Model

In the firstly proposed LIP model [3], [12], the intensity of an image is completely modelled by its gray tone function u (which has the physical interpretation of an absorption function), with $u \in [0, D)$. The usual convention is that D represents the maximum absorption (perfectly black image) while 0 represents the total reflective object. In the LIP model, the addition of two gray tone functions u and v and multiplication of u by a real number λ are defined in terms of usual $\mathbb{R}$ operations as:

$$u \oplus v = u + v - \frac{uv}{D} \tag{2.8}$$

and respectively:

$$\lambda \otimes u = D - D\left(1 - \frac{u}{D}\right)^{\lambda} \quad . \tag{2.9}$$

The underlying isomorphic function is:

$$\Phi_J(x) = -\log(1 - x). \tag{2.10}$$

2.2.2 Pătraşcu Model

The logarithmic model introduced in [13] works with bounded real sets: the gray–tone values of the involved images, defined in $[0, D)$, are linearly applied onto the standard set $(-1, 1)$. This interval plays the central role in the model: it is endowed with the structure of a linear (moreover Euclidean) space over the scalar field of real numbers, $\mathbb{R}$. In this space, the addition between two gray-levels, u and v is defined as:

$$u \oplus v = \frac{u + v}{1 + uv} \tag{2.11}$$

while the multiplication of a gray level, u with a real scalar, $\lambda \in R$ is:

$$\lambda \otimes u = \frac{(1+u)^{\lambda} - (1-u)^{\lambda}}{(1+u)^{\lambda} + (1-u)^{\lambda}} \quad . \tag{2.12}$$

The underlying isomorphic function is:

$$\Phi_P(x) = \frac{1}{2}\log\frac{1+x}{1-x}. \tag{2.13}$$

2.2.3 Vertan Model

A later proposal for such model is the so called "pseudo-logarithmic" model proposed by Vertan et al., [5], [8].

The pseudo-logarithmic model restricts the gray tone definition to $E = [0, 1)$ range. The addition of two gray levels, u and v, is defined as:

$$u \oplus v = 1 - \frac{(1-u)(1-v)}{1-uv} \tag{2.14}$$

and the multiplication with a scalar constant, α is:

$$\alpha \otimes u = \frac{\alpha u}{1 + (\alpha - 1)u} \tag{2.15}$$

The underlying generating isomorphism is:

$$\Phi_V(x) = \frac{x}{1-x}, \tag{2.16}$$

while its inverse function is:

$$\Phi_V^{-1}(y) = \frac{y}{1+y}, \tag{2.17}$$

As observed from the equation (2.16) above, the proposed homomorphic function is not logarithmic, but it closely mimics that behavior, which justifies the "pseudo-logarithmic" name used for this model. By comparison, the Jourlin–Pinoli and Pătraşcu models use logarithmic generative function.

If discussing the mathematical structure of models, since the generative functions of the Jourlin–Pinoli and Vertan model are defined over asymmetrical sets, the structure is of a cone space. Only Pătraşcu model has, truly, a vector space structure.

2.2.4 Piecewise Linear Model

The exercise developed in section 2.1, beyond pointing to a short-cut to the mathematical analysis of known models, gives the user the flexibility to choose the generative function according to his application particularities. Here, we shall investigate a general problem. All of the known models share the same complex behavior, which leads to the practical problem of lack of efficiency in implementation [14]. Hence, it make sense to try to build a piecewise linear model. Thus, we shall choose a piecewise linear generative function that complies with the rules determined in section 2.1 and we derive the remaining of the model later.

Let us consider a generative function composed of n segments. Such a function and its inverse have the form:

$$\phi_L(x) = \begin{cases} a_1 x + b_1, & x \in [x_1, x_2) \\ a_2 x + b_2, & x \in [x_2, x_3) \\ \dots \quad \dots & \\ a_k x + b_k, & x \in [x_k, x_{k+1}) \\ \dots \quad \dots & \\ a_n x + b_n, & x \in [x_n, x_{n+1}) \\ +\infty, & x \in [x_{n+1}, +\infty) \end{cases} \tag{2.18}$$

and respectively:

$$\phi_L^{-1}(y) = \begin{cases} \frac{y-b_1}{a_1}, & y \in [y_1, y_2) \\ \dots \quad \dots & \\ \frac{y-b_k}{a_k}, & y \in [y_k, y_{k+1}) \\ \dots \quad \dots & \\ \frac{y-b_n}{a_n}, & y \in [y_n, y_{n+1}) \\ x_{n+1} y \in [y_{n+1}, +\infty) \end{cases} \tag{2.19}$$

In the equations above, the offset (intercept) constants, $b_1, b_2, \dots, b_n$, are determined from the continuity constraints imposed to both of the functions.

In order to determine the operational laws, one will replace the generative and inverse generative function formulas (eq. (2.18) and (2.19)) in equation (2.1). The proposed model is function of the $a_1, a_2, \dots, a_n, x_1, x_2, \dots, x_n, x_{n+1}$ parameters. To determine their values, one may choose a non-linear model as target and perform parameter regression. But in section 2.1 we showed that it is no need to do that, because the known models span just a little part of the valid functions range. We have some degree of freedom in choosing the parameter set according to the envisaged application. For instance let us aim at efficient implementation. We consider the choice of line slopes $a1, a2, \dots, a_n$ as power of 2 as being more important, such that the model implementation uses bit shift instead of the expensive multiplication and, especially, division. Under such an approach, the abscissa breaking points, $x_1, x_2, \dots, x_n, x_{n+1}$, is a free parameter and is to be found after minimizing the mean squared error (or other similar criteria) in respect to a target model. We stress that given a number of segments, n, the parameters are to be found once in an off-line calculus and used straight–forward in practical real-time applications.

2.3 The Generating Function as Composite Function

The basic result that allows us to extend the NIP (LIP) models comes from the algebraic theory [15]. It states that the composition of two valid homomorphisms leads to another homomorphism. Let be $\psi : E_1 \to E_2$, a homomorphism from E_1 to E_2 and let $\phi : E_2 \to F_2$ be a homomorphism from E_2 to F_2, then the composite function $\rho = \phi \circ \psi = \phi(\psi) : E_1 \to F_2$ is a homomorphism from E_1 to F_2. Under such a construction we choose ϕ to be the generative function Φ of a known NIP model, while ψ may be a real function with bounded domain and target set and the result is a valid new NIP model. One may go even further: it is not really necessary to have the ψ function a homomorphism, but only bijective function; even in such a case the results is a valid generative NIP model function.

Examples of such bounded bijective function may include:

- linear transforms: $\psi(x) = ax, a \in \mathbb{R} - \{0\}$;
- afine transforms: $\psi(x) = ax + b, a \in \mathbb{R} - \{0\}, b \in \mathbb{R}$;
- power function: $\psi : [0,1] \to [0,1], \ \psi(x) = x^m, m \in [0, +\infty)$;

2.3.1 Parametrization

The parametrization is naturally achieved if the ψ function is a parametric function and in all the cases uses the same sets. Such an example may be the family of "power-type" functions:

$$\psi_m : [0,1) \to [0,1), \ \ \psi_m(x) = x^m, \forall m \in (0, +\infty) \tag{2.20}$$

We note that all members of this family are bijective functions.

For instance, if we compose this family of functions with the generator mapping of the pseudo-logarithmic model, one will obtain a set of parametric NIP models. The base function is:

$$\begin{aligned} &\Phi_m : [0,1) \to [0, +\infty), \\ &\Phi_m(x) = \Phi\left(\psi_m(x)\right) = \frac{x^m}{1 - x^m} \end{aligned} \tag{2.21}$$

The inverse function is:

$$\Phi_m^{-1}(y) = \psi_m^{-1}\left(\Phi^{-1}(x)\right) = \sqrt[m]{\frac{y}{1+y}} \tag{2.22}$$

The mathematical formulas of the so-generated model are found if one replaces formulas (2.21) and (2.22) in equations (2.3) or (2.4). For example, the general formula for addition, $\oplus_m$ becomes:

$$\begin{aligned} u \oplus_m v &= \psi_m^{-1}(\psi_m(u) \oplus \psi_m(v)) \\ &= \sqrt[m]{1 - \frac{(1-u^m)(1-v^m)}{1-u^m v^m}} \end{aligned} \tag{2.23}$$

where $\oplus$ is, in this case, the pseudo-logarithmic addition.

We have to note that the "power" function is the hereby choice and any other bijective parametric function will do. This family of functions is appropriate for means of exemplification, since it includes convex functions (for $m > 1$) as well as concave ones (for $m < 1$) and different behaviors are at hand. For $m = 1$ the pseudo-logarithmic model is retrieved.

Chapter 3

Digital Still Camera

Historically the photography counted more than 150 years of evolution. Lately, the technological advance pushed the photography in the digital era. In this chapter on overview of the most important constructive features of the digital still cameras will be provided.

The nowadays digital cameras may be classified in two categories: single-lens-reflex (SLR - professional and expensive) and consumer (cheaper but less qualitative). However the construction of both types implies the use of several blocks:

- Optical System;
- The image sensor;
- The post processing image core.

If the optical system goal is to focus the scene image as good as possible on the image sensor, the undesired effects of a less qualitative system are geometrical artifacts. However, because the geometrical distortions of the image are beyond the range of the current study, we shall only remind their existence and avoid detailing them.

3.1 Image Sensor and Exposure

The camera's photo-detectors (which may be of CCD or CMOS type) act according to an accumulative law. The incident light $\lambda(t)$ is integrated over the exposure time, T_{exp} to produce the reported output intensity:

$$\Lambda(T_{exp}) = k \int_0^{T_{exp}} \lambda(t)dt \ , \tag{3.1}$$

where k is a system constant. An insight over this constant is given by the APEX equation, which binds the exposure time, aperture and the incident light:

$$EV = -\log_2(T_{exp}) + 2\log_2 N = \frac{\Lambda \cdot S}{K} \ , \tag{3.2}$$

where EV is the exposure value, the log of T_{exp} forms the time value (TV), N is the relative diaphragm opening (by taking the log, the aperture value, AV, is formed), Λ is the cumulated incident light, S is the sensors sensibility (or for digital cameras - the amplification) and K is a known constant (given by the specific of the camera).

Once the intensity of the light has been acquired in analog form, analog to digital conversion must take place. Conversion to 12 bits is common for consumer camera, while professional ones may go up to 14 bits. The currently digitized image is in the "RAW" format, in the sense that one pixel stores only one component of color (red, green or blue), which corresponds to the color filter placed in front of the original photo-detector. The spatial distribution of colors typically follows the Bayer format, [16], implying that it uses twice as many green pixels as red or blue.

3.2 Image Processing Algorithms

In order to transform the RAW image into one that may be shown on common displays a set of image processing algorithms have to be implied. This set includes:

- De-noising and biasing;
- De-mosaicking - which completes the color for all pixels, but often with reducing the color depth to 8 bpp;
- White balance - which tries to compensate for color deviation introduced by the light source;
- Gamma correction - which adapts the image to the non-linear behavior of the typical CRT display

The main idea is that the set of image processing algorithms implied by the camera transforms the final image into a non-linear replica of the intensity subject image. Instead of accurate determination of the effect of each such block, it is common to model the camera as a black box described by a function called Camera Response Function (CRF) or camera transfer function (CTF).

3.3 Estimation of Camera Response Function

The subject of estimating the camera response function has been widely debated in literature. The first attempts were based on taking a single exposure of the uniformly illuminated chart containing patches of known reflectance, such as the Gretag Macbeth chart [17]. The Gretag Macbeth Color Checker provides a subject scene with uniform patches and intensity varying over the entire range of interest. The CRF is estimated in the given set of brightness values and interpolated in the rest. However, the process is quite complicated and can only be performed in restrictive conditions (e.g. the environment illumination must remain un-changed), which are not always accessible.

Later attempts were based on the Debevec and Malik observation, [18], which states that a set of differently exposed images contain, usually, enough information to recover the CRF (denoted here by g) using the images themselves.

If the scenario conditions include the same scene, aperture number and sensors amplification as constants, then, by taking into account the right term of equation (3.2), the measured intensity is linearly dependent of the exposure time. To be more precise, let us assume that images A and B of the same scene were photographed with different exposure times t_A and, respectively, t_B. Given a photo-detector, its charge from the two images must preserve the same ratio as the exposure time. Now, if we come to the reported pixel values u_A and u_B, we get the basic CRF equation:

$$g(u_B) = \frac{t_B}{t_A} g(u_A) \ . \tag{3.3}$$

Recovering g from the equation (3.3) is a difficult task, [19]. Certain restrictions have to be imposed on g. The minimum irradiance, 0, will produce no response of the imaging system, hence $g(0) = 0$. The maximum irradiance is an unrecoverable parameter, but the sensors output is limited by a saturation level in the photo-detectors, $u_{\max}$, therefore there is an upper-bound : $g(u_{\max}) = D$. The monotonic behavior of g is, also typical assumption. Mann and Picard, [20], proposed a gamma-like function for g, while Mitsunaga and Nayar, [21], used low degree polynomial regression. Debevec and Malik [18] used a smoothness constraint and recovered the response using non-parametric model of g, sampled at certain values, and represented it by a vector.

3.3.1 Logarithmic Multiplication

An alternative to estimate the exact values of a digital camera transfer function is an approximation of the variation of exposure by using the multiplication according to the logarithmic model proposed by Jourlin - Pinoli.

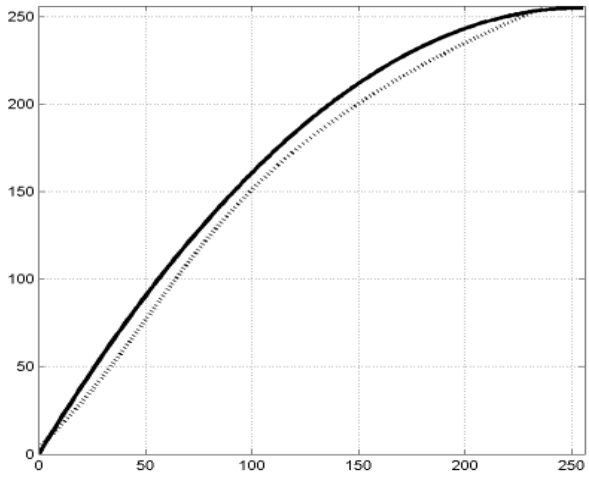

Figure 3.1: Transfer function approximation for a consumer digital camera (with dotted line) compared with amplification of the Jourlin – Pinoli model, presented with continuous line.

The starting point in this approximation lies in the fact that photographic film was built to follow the Weber law. This law, [22], describes the response of the human eye to a linear variation of the stimulus as being logarithmical. The consistency with the Weber law is one of the properties of the LIP model proposed by Jourlin – Pinoli, as showed in [23]. Once the digital camera had come out, they have followed the same pattern as their film counterparts; this implied the non-linear response characteristic.

Thus, as been showed in [24] and [25], we should expect minimum differences between a camera CRF and logarithmic scalar multiplication. This statement is proved by the example showed in in figure 3.1.

Chapter 4

Under–exposed Image Amplification

Not too long after their appearance in the early 90's, digital still cameras (DSC) have become the common way of acquiring images. Nowadays, the main direction seems to be that of decreasing the size and weight of imaging devices, which has reached a pinnacle with Mobile Phone Cameras (MPC). At the same time the camera producers engage with tremendous efforts in the Megapixels race.

The trend of miniaturization mentioned above is imposing design modifications such as reducing the size of optics and of photo-sensible area. If we discuss these issues from an end-user point of view, the problem is that of increased susceptibility of images to blur from shaking hands [26]. The small photo-sensible area diminishes the number of collisions in the photo-voltaic effects and, therefore, it reduces the correlation between the incident light and the reported image intensity. On the other hand, the small photo-sensible area decreases picture angle. Since human hand jitter is always present, [27], the small picture angle increases the chances that the relative motion between the camera and the scene during exposure time becomes larger than a pixel size and thus leading to visible motion blur.

Since this phenomenon can significantly degrade the visual quality of images, photographers and camera manufactures are frequently searching for methods to limit the effects. This problem has been widely studied and academic literature and industrial research abounds with attempts to deal with it. We may divide these approaches in two categories. This first approach tries to eliminate the effects of the motion blur, meaning that there will be a normal image acquisition (with a long enough exposure time that includes blur) and subsequently camera trajectory is estimated in order to restore it. The restoration and the estimation processes may be simultaneous and real-time (the so-called

optical image stabilization, [28]) or consecutive and digital (by means of de-convolution, [29], [30]). However this alternative implies the use of motion sensors (which came as an extra circuit) and therefore contradict the size-diminishing goal.

The second approach works on avoiding the circumstances that generate motion blur. This is achieved by reducing the exposure time below the "motion limit". The motion limit may be based on the "q over f35" rule of thumb [31] or dynamically deduced from computing the misalignment on consecutive frames for more precise indication of camera motion [32]. This alternate solution may be easily implemented on existing digital camera hardware, without any effects on size. However, if such a solution is chosen, the under-exposed image must be amplified so to provide proper luminance and color saturation level. The problem implies multiplication of a given image to a desired one. The multiplication must avoid introducing image artifacts that will decrease the perceived image quality. We will focus on this solution and, as it was shown in section 3.3.1, the use of Logarithmic Image Processing Model or, by extension, of any NIP model provides means for solving the mentioned problem.

4.1 The Amplification Algorithm

A typical low-light enhancement method firstly captures an image with a short exposure time. This image is hand motion free but under-exposed. Next, the image is amplified until its luminance and color levels match that of a reference. The reference may be intrinsic (e.g. as the one provided by equation (3.2) with a large value for ISO parameter S) or it may be an external one, (other image as described in [33]).

The reference in the latter approach is a correctly exposed image, which may be blurred. This provides additional information than a single number derived from equation (3.2). For the currently proposed solution, an important demand is the relative short period between the capture moments of the two required images: the reference and the main image. This helps prevent large geometrical misalignments and, hence, avoid the time-consuming image registration (as is the case of [33]). Such a demand is easily met in the case of the CMOS sensors where consecutive read-out may be taken without discharge of the image sensor [34].

Now, let us denote the main, low-light, image, which is of $N \times P$ resolution with $F(i,j)$ with $i = 1, \dots N$ and $j = 1, \dots, P$. The reference image (which we shall denote by $G(i,j)$) may have the same or a lower resolution than the subject image. If different

resolutions are implied, one may a use a nearest neighbor interpolation to even the image sizes (to the high resolution $N \times P$).

The enhancement method works in two steps; first, it performs a rough global amplification; later, it refines individual pixels by taking into consideration local information. In the following paragraphs, we shall proceed with describing the actual method.

Given the two images, G and F, the rough amplification is performed by considering a reduced set of (spatially matching) pixels from each image: $G_S \subset G$ and, respectively $F_S \subset F$, and by means of linear regression, computing a pair of coefficients, c_1 and c_2, [35], so that:

$$G_S \approx c_1 F_S + c_2 \tag{4.1}$$

The image computed using the coefficients from equation (4.1), $F_1 = c_1 F + c_2$, corresponds in most cases with the standard (simple reference) amplification methods. However, we must observe that the results are highly dependent on the choice over the set of reduced pixels, which may or may not be representative for the image. If full resolution image is used then blur artifacts may be transferred from the reference image to the main image. Furthermore, if classical real addition and multiplication are used in equation (4.1), the result is sensitive to range overflow. Therefore, an implementation based on non-linear amplification (which let us remember that is closed) is more practical.

The second step of the enhancement, the fine amplification is performed locally, in the sense that different amplification factors are used for different pixels. To be more explicit, we shall determine the matrix $W(i, j)$, with $i = 1, \ldots N$ and respectively $j = 1, \ldots P$, so that:

$$F_2(i, j) = W(i, j) F_1(i, j), \forall i, j \tag{4.2}$$

The computation of W's coefficients relies on the 1-D adaptive filtering theory which has the obvious advantage of being computationally efficient. The actual implementation implies the use of a filter with a single adaptive coefficient. But first the 2-D images are turned into 1-D vectors by arranging them in lexicographic order:

$$\{W(i, j), F_1(i, j)\} = \{W(k), F_1(k)\}, \;\; k = (i - 1)P + j \tag{4.3}$$

The equation that updates the filter is taken from sign-data LMS (Least Mean Square) algorithm and it makes use of the fact that the input data, $F_1(k)$ is always positive:

$$W(k + 1) = W(k) + \mu(k) e(k) \;\; , \tag{4.4}$$

where $\mu(k)$ is the step size (fixed or variable), the $e(k)$ is the error signal computed as:

$$e(k) = G(k) - F_2(k) \tag{4.5}$$

For accurate implementation, one may use a fixed step size $\mu(k) = \mu = 0.005$ and it may initialize the filter value with multiplication neutral element $W(1) = 1$.

As previously discussed, if standard multiplication is used in equation (4.2), range overflow situations are often encountered in highly illuminated areas. Furthermore, in the same hypothesis of linear amplification, if one will extend the method to color (multi-planar) images by replicating the algorithm for each color plane, the resulting image will have over-saturated colors. In order to prevent these problems we are using non-linear scalar multiplication.

Practical implementation tends to simplify the described method. To be more precise, a single coefficient may be used in the rough amplification, eq. (4.1) and a set of reduced possible values for the fine scaling constant; hence we are able to express the multiplication by look-up table.

4.2 Results

For demonstration purposes, we considered a low-light scene containing the Gretag Macbeth Color Chart placed on a wooden support. The input images (main and reference image), as well as the results may be seen in figure 4.1. The reference (4.1 subplot (b)) and main image (4.1(a)) were obtained with a consumer camera held in the hands; thus they are susceptible to motion blur. The under-exposed subject image (4.1, (a)) was obtained by forcing the exposure value to be $EV = -2$. The ideal image (which is not affected by motion blur) was recorded with a tripod mounted camera. As results, we showed our image (d), the image obtained by described amplification but performed in a linear space (e) (which is obviously over saturated in the upper part - the wooden support) and respectively the subject image processed by typical auto-contrast and auto-saturation algorithms (f). The last possibility is well known and it is used in the world of amateur photographers; its result suffers from poor color reproduction. Concluding, it is easy to observe that the best results are obtained by using the two step logarithmic amplification.

Furthermore, we considered an extensive testing procedure, with three scenarios (our method with logarithmic and respectively linear amplification which includes larger data

Figure 4.1: (a) Under-exposed subject image; (b) Motion blur-degraded reference image; (c) Ideal image; (d) Logarithmic amplified image; (e) Linear amplified image; (f) Auto-Contrast Image.

sets, with different scenes, but under the constraint that there is no misalignment between the ideal image and the resulting ones. Under these circumstances, we were able to compute a Normalized Mean Square Error. A short summary of the results may be seen in Table 4.2. As one can see, the results are degrading if we underexpose more; however the logarithmic amplification provides the most reliable results in all conditions.

	LOG	LIN	Auto
EV =- 1	0.0053	0.0214	0.0120
EV =- 2	0.0063	0.0254	0.0182

Table 4.1: Values of the NMSE for the logarithmic amplification (LOG), linear amplification (LIN) and auto-contrast(Auto) if the low-light image was under-exposed with EV=1- or EV=-2 stops

The method has limited performances in case of underexposed images with more than EV=-2 (the signal is low enough and noise is amplified) or in the case of sizeable misalignment between acquired images (our test showed a value of 30 pixels for 5Mpixel image as the maximum acceptable misalignment). Under such conditions even if our method is the most reliable, it does not pass a visual inspection. As described, the method is most suitable for software implementation and most of in-camera processors can handle the computation. Hardware implementation is possible, but due to method simplicity, the cost of building dedicated chips may not be compensated by speed improvement.

This method has been described in US patent [34] and in the paper [24]. The method is part of the package of commercial applications developed by the Smart Imaging division from Tessera and covered by the mentioned patent.

Chapter 5

Dynamic Range Enhancement

Most real-world images seen by the human eye contains an impressing number of colors. Typically, digital camera sensors can capture a lower value dynamic range (in the order of 256), while the human eye, according to the experiments lead by Blackwell [36] can distinguish up to 10000. Therefore, under certain circumstances there is need for algorithms that enhance the dynamic range of images acquired by digital still camera.

The straightforward solution to the problem generated by the reduced dynamic range of digital still cameras is to combine multiple images of the same scene, taken under various settings (exposure time, aperture). This approach is generally known as bracketing or HDR algorithm. The underlying idea is that each of the images that are to be combined captures with high quality only a certain part of the scene gamut. The bracketing algorithms select, for each pixel of the spatial support scene image, the combination of frames that provide the best value. That selection is based on the assumption that the multiple images are perfectly aligned. Thus, an implementation of the dynamic range increase works in several steps: a first step of image acquisition followed by a possible registration level (that aligns the multiple images captured from the scene), a step of camera response function estimation and the actual image combination (fusion, or pixel value selection), that computes the enhanced image.

5.1 Image Acquisition

The requirement for the input images is to have been captured under different exposures. Taken into account the special features of digital cameras light acquisition, several solutions are at hand:

- Varying exposure time. This is the most used method. The drawback lies in differences of content between the frames, which may appear for a hand-held camera or for a scene with moving objects.

- Varying aperture. Since aperture variation leads to different depth of the image, this solution is usable only for planar images.

- Varying camera scaling constant. This may be achieved either by varying the photo-sensible area as in the case of Fuji Super CCD, [37], or by varying attenuation of the optical system, as proposed by Nayar et. al, [38]. Unfortunately both solution requires constructive modifications.

In conclusion, the most likely approach to be used, especially for static scenes, is to vary the exposure time of the individual images. In such a case a step of image registration may be required.

5.2 Image Registration

Image registration means the geometrical alignment of multiple images of a scene, based on the matching of the content. Image registration is a widely dealt issue in the field of image processing and several solutions (block matching methods, edges matching methods, object matching methods or global matching methods) are at hand [39].

The most performing method is considered by many as being the block matching method. Here, both images are divided in disjoint blocks and each block from the subject image is searched in the reference image. A criteria that identifies the best match must be implied. Typical choices are the minimum of sum of absolute differences, the minimum of sum of squared differences, the maximum of inter–correlation [40]. However full search of blocks is rather costly from the implementation point of view and simplified methods came out. Sauer & Schwartz, [41], turn the bi-dimensional problem in two one-dimensional problems by computing the image projection on two axis and applying a known registration technique. Albu et. al., [42], move even further, and consider the orthogonal projection onto a space with binary values.

An alternative to these methods consists from the robust global matching method of spectrum phase correlation [43], [44]. The underlying idea is based on the translation property of the Fourier transform, $\mathcal{F}$: a translation in the spatial (or time) domain t of a

signal x yields a phase shift in the transformed domain.

$$\mathcal{F}\left[x(t+t_0)\right](\omega) = \mathcal{F}\left[x(t)\right](\omega) \cdot e^{-j\omega t_0} \ . \tag{5.1}$$

Therefore, for a pair of non-aligned images, one will find the corresponding shift as the maximum difference in the phase spectrum of the images. However, the method is designed to perform only if the images exhibit a similar content and if there is no rotational misalignment. Our experiments showed that this method is a good compromise between accuracy of results and efficient computation.

5.3 Image Fusion

5.3.1 Simple Fusion

The image fusion step is the actual dynamic range increasing procedure. A simple approach for fusing a set of N frames taken by a digital camera under several exposures is to discard the pixels with saturated values and to average the remaining values [45]. The frames, denoted by $f_1, ..., f_N$, are corrected by the exposure factor $EV(i)$, such that the pixel located at coordinates (l, m) in the resulting image, is obtained as:

$$f_{HDR}(l,m) = \frac{1}{N_0} \sum_{i=1}^{N_0} 2^{EV(i)} \cdot f_i(l,m) \ , \tag{5.2}$$

where N_0 is the number of frames having non saturated values at the specified location.

5.3.2 Image Weighting

It is not feasible to assume that independently of the frame exposure value, the camera outputs the scene brightness correctly. For over–exposed pictures, it is less likely that pixels having values near the saturation level are accurately recorded. For under–exposed pictures, values from the lower part of the range suffer the noise influence and their reported value is corrupted by quantization errors. Instead of precise determination of the g function, as in the other mentioned approaches, we will simply compute the confidence that we have in a value given an exposure value.

There are different pairs $\{T_{exp}, N\}$ (exposure time - aperture) that satisfy equation (3.2). Most of the digital still cameras available on the market are capable of estimating the deviation of the exposure value from the set that balances equation (3.2). Thus,

multiple scenes with the same EV may be obtained; averaging the results will decrease the error of estimation.

Given an exposure value, an image of the usual Macbeth Color Checker chart should exhibit a known set of values. In reality, the camera outputs different brightness intensities. The sum of the squared differences between the output values and the expected values normalized by the expected value is used a measure of error, ε. A low order polynomial regression is implied to extend the domain of the error function from the 24 original values (the number of patches in the chart) to the [0,255] required range. The error function is represented as matrix were the rows are bind to the exposure value parameter, while the columns span the possible gray-levels: $\varepsilon \to \varepsilon(EV, u)$. The confidence function is computed similarly to a fuzzy negation from the globally normalized error functions:

$$\mu(EV, u) = 1 - \varepsilon(EV, u) \ , \tag{5.3}$$

where, again, EV denotes the exposure value and u denotes the gray level.

An example of normalized confidence functions computed on images acquired with a consumer camera are shown in figure 5.1.

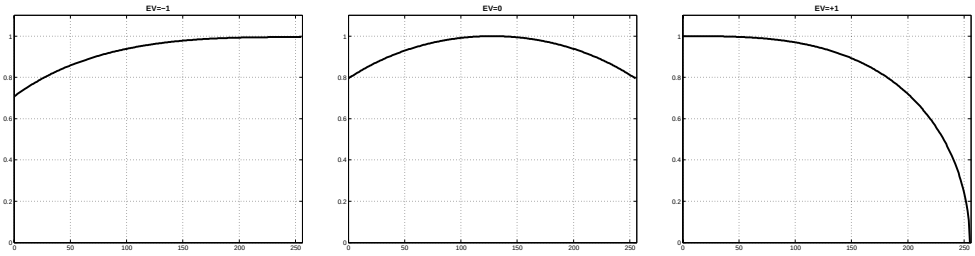

Figure 5.1: The plots of the μ function in respect to the $[0, 255]$ gray levels for $EV = -1$, $EV = 0$, $EV = 1$.

Taking into account the confidence value computed in the previous subsection, a more informative approach is to consider the weighted average (or the convex combination of the pixel values). The weights encode the confidence that a value is outputted correctly. By this approach, the resulting image is computed as:

$$f_{HDR}(l, m) = \frac{\sum_{i=1}^{N} \mu\left(EV(i), f_i(l, m)\right) \cdot 2^{EV(i)} \cdot f_i(l, m)}{\sum_{i=1}^{N} \mu\left(EV(i), f_i(l, m)\right)} \ . \tag{5.4}$$

5.3.3 Non–linear Image Fusion

An alternative to the real operations used in equation (5.4) is to use operations extracted from non-linear image processing models, [9], [10]. The multiplication of an image level with the associate weight and respectively the normalization follows a particular model (Jourlin–Pinoli, Vertan, piecewise linear) of the equation (2.4), while the addition from the sum follows equation (2.3)

The advantage of using NIP models is the dynamic range reported by the resulting images. If one will examine equation (5.2) with $N_0 = 2$ and the inputs being all possible combinations of pairs defined between 0 and D, then there will be $2D-1$ possible resulting levels. If the operation is performed using equation (2.8) - Jourlin–Pinoli model for instance, then the number of outputted different levels is in the order of $\frac{D^2}{4}$, while equation (2.11) leads to a order of $\frac{D^2}{2}$. The non-linear addition produces an over-sampling of the output values space. The corresponding dynamic range value for $D = 256$ is, roughly: $DR = 10 \log\left(\frac{D^2}{2}\right) \approx 45dB$, compared with $24dB$ for a single image or 28 dB for real–based operations.

Thus, implementing the image fusion in a logarithmic space (or, shortly, by applying log-bracketing) the resulting image will exhibit largely increased number of different brightness levels (which can give the user the possibility of detecting objects in uniform areas from the original images).

5.4 Results

One application of the current method is for natural images. Another application which, from a certain point of view is more important, is dynamic range extension for digitizing analog radiographs.

For evaluation of the results two methods are at hand (and the corresponding results are to be seen in table 5.4). One method is the subjective evaluation, where a set of observers, expert and non-expert graded the resulting images from worst quality (0) to the best quality (5).

The other method regards an objective score and that is implemented as entropy effectiveness. Given the specific requirements of the tested application (HDR enhancement), we claim that pixel values entropy can be used as an objective measure because a HDR image must allocate comparable portions of the visible range to all objects; in such a case,

Method	Gray–level		Color	
	ρ_s	MOS	ρ_s	MOS
I_{EV-1}	0.203	-	0.125	-
I_{EV0}	0.150	-	0.112	-
I_{EV+1}	0.136	-	0.156	-
Simple	0.293	3.75	0.110	4.25
Jourlin–Pinoli	0.121	4.75	0.087	4.75
Vertan	0.125	4.75	0.100	4.37
Piecewise Linear	0.144	4.50	0.112	4.25

Table 5.1: Evaluation measures of HDR images for gray-level and color images set by entropy effectiveness, ρ_s, and Mean Opinion Score, MOS, (the average grade of the human observers).

the information (which is measured by entropy) should be maximum. Indeed, as we expect, the HDR image exhibits the maximal range of values, their distribution resembling a uniform one. We measure the entropy effectiveness as:

$$\rho_s = 1 - \frac{H(F)}{H_{\max}(f)} \tag{5.5}$$

$$H(f) = -\sum_{u=1}^{D} p_i \log p_u \quad \left[\frac{\text{bit}}{\text{symbol}}\right], \tag{5.6}$$

where p_i is the luminance histogram value corresponding to gray level i and M is the maximum number of different pixel values. The maximum value of the entropy is the number of bits per pixel.

The first observation is that the entropy, which is a measure of the uniformity of the image histogram, is consistent with subjective evaluation. The next observation is that the Jourlin–Pinoli model is the most appropriate for the current experiment followed closely by the Vertan model. The piecewise linear model (used here with 5 segments) is a reasonable compromise.

5.5 Dynamic Range Enhancement for Analog Radiographic Images

A result with high practical utility of the HDR algorithms is found in the digitization of analogue radiographs. The importance of such contribution is enhanced by the fact that medical imaging results act directly on the humans. By medical imaging means, the clinician sees inside the patient. If the investigated part is the human skeleton, then the typical mean is by X-ray machine and radiographs. Modern analysis techniques, due to the use of computer assisted diagnosis requires data in digital format. Unfortunately the digital X-ray machine became available only in recent times and even now, the orthopedic and radiologic centers from remote areas are using analogue (film) devices. So the analogue to digital conversion problem still holds.

To enhance the need of digitization we shall add the problem of specialists. Not in all the medical centers with analogue X-ray devices there are highly qualified doctors and, now, for complicated diagnosis the film radiograph has to be physically transported to the advanced center. A digital image can be sent over data connections and the diagnosis process and treatment will be highly speed up, [46].

The problem of digitizing analog radiographs may be addressed in two ways: with performing scanners or with digital cameras. The first solution may be more easy but is also more expensive. The digital camera solution is cheaper, especially if consumer ones are used, but it has the drawback of decreasing the dynamic range from the 12 bits of the analogue film to the 8 of the digital image. Hence a dynamic range enhancement method, that will ensure that all the input information is preserved, is needed.

An initial solution of extending the dynamic range of camera acquired images of analog radiographs makes use of the total ordering method, described in [47]. It has the advantage of requiring only one input image. However, as discussed in [48], better results are retrieved if more input images, each accurately recording different parts of the high gamut, are used. Our proposal, validated against medical personnel opinion, is the so called log-bracketing method, which implies several images, weighted in respect to each pixel accuracy, [49], followed by image fusion based on non-linear operations, [9], [10]. The next, future, step of this algorithm is to build a certified standard of digitizing analogue radiographies.

Once that informative digital images are at hand, analysis techniques may follow. For

instance, we focused on the analysis of the prosthesis fit inside the the femoral channel in the case of the total hip arthroplasty. Following digitization, segmentation techniques separate the prostheses from the femoral bone and a score of the fit is computed, [48], [50]. The schematic of the full system may be followed in [51]. In [52], a 3D model of the local bone system is build for visualization and further analysis purposes, while in [53], the bone texture analysis is explored; here accurate digital information is required for accurate analysis results.

Chapter 6

Conclusions and Future Work

This work focussed on studying a set of non-linear processing applications for enhancing images acquired with digital still cameras. If the origin of the work lies in the logarithmic image processing models, the shared feature of the proposed applications is that the input data was recorded with a digital still camera.

Regarding the logarithmic image processing models, we try to sought the answer to the question: "Are there any other models of those known?". In order to solve this dilemma, in Chapter 2, it was needed to make a call to mathematical instruments from the algebraic theory of homomorphisms and vector (cone) spaces, instruments otherwise fairly simple, so with great potential for practical impact. Thus, we found a set of sufficient conditions that if fulfilled by a function that is to be applied to the real space structure, will lead to determination of a new non-linear model for image representation and processing. The new model will have a structure of vector/cone space. Between the described applications, parametrical models and piece-wise linear ones have been presented.

But the hereby paper aims to be a work in a field of engineering sciences, so the theoretical discussion about the logarithmic models expansion in the area of models generated by non-logarithmic functions is doubled by two applications. Both applications, although at first sight on a different objective, are dedicated to images acquired with digital still cameras.

In fact, the way light is processed in cameras, which is deeply non-linear, was the unifying grip of the applications. The first of the two applications is related to amplifying images with a time of exposure under normal value. The algorithm developed for solving the mentioned problem, described in Chapter 4, can be used as a solution to the extremely pressing problem of degradation by blur of photographic images due to human hand

jitter. This application is developed by a research group that includes the author, for the company Tessera and has attracted great public interest in the most important exhibitions dedicated photographic techniques (PMA 2008). This product will be publicly launched, probably, during 2009.

The second application, with the largest share in the work, relates to expanding the dynamic range images acquired by digital cameras. The proposed solution, the so called "log-bracketing" algorithm, firstly weights the acquired frames, so later to non-linear fuse them and, therefore, to greatly enhance the resulting image dynamic range. This application has in view both the images of natural colors and gray–level more particularly in the process of digitizing analog X-rays. In fact a group of researchers from the University "Politechnica" of Bucharest and University of Medicine and Pharmacy "Carol Davila" has aimed to standardize a low cost method for transferring digital information stored on analog X-ray film. Such a standard opens the way for digital processing and analysis algorithms to images from analog databases accumulated in the span of decades of clinical investigation of human skeleton. Going further, such a standard, in conjunction with digital image transmission via existing data networks open access of the remote centers to highly qualified and experience clinicians from large medical centers.

6.1 Future Work

Boundaries that were broken in the generating of non–linear image processing and representation model require further investigation. The multitude of applications already developed on the basis of (pseudo)logarithmic models can benefit from greater flexibility of parametrization. The speed of calculation can be increased without loss of quality with the piece-wise linear model. The replacement of addition or of scalar multiplication in an existing application with excerpts from a new model, or possibly one that will be derived at the right time, can lead to results of a high quality if the model has specific properties that are closer to the requirements. In terms of theoretical analysis of the nonlinear models for images representation and processing, although with substantial contribution, this work has not exhausted the subject because only sufficient conditions were determined, while the necessary ones not yet.

Regarding the solution proposed to reduce the blur in digital photography, they include a future release to the public. Only time to come will show if this solution will have the same impact for ordinary user that had on the community in the field.

The method proposed for extending the dynamic range of digital photos is a step in a more complex system. As can be seen in the attached bibliography, the research of the hereby author in this area is closely related to X-ray zone of hip. For these cases the model proposed by logarithmic Jourlin – Pinoli provided the most elaborate solution, and the Vertan model was the ideal compromise between complexity and efficiency of calculation. Based on these images were constructed systems of analysis which are demonstrating their value in a medical point of view. On the other hand, if in future, focus will be other parts of human skeleton out of the balance area, further analysis of the acquisition system is needed to find out what model is most suited in the enhancement of dynamic range.

Bibliography

[1] A. V. Oppenheim, *Superposition in a Class of Non-Linear System.* Cambridge, U.S: Research Laboratory of Electronics, M.I.T., 1965.

[2] J. Lim, *Two Dimensional Signal and Image Processing.* New Jersey, U.S: Upper Saddle River, Prentice Hall, 1990.

[3] M. Jourlin and J. C. Pinoli, "A model for logarithmic image processing," *Journal of Microscopy*, vol. 149, no. 1, pp. 21–35, 1998.

[4] V. Pătraşcu, "Modele matematice pentru prelucrarea logaritmică a imaginilor," Ph.D. dissertation, Universitatea "Politehnica" din Bucureşti, 2001.

[5] C. Vertan, A. Oprea, **C. Florea**, and L. Florea, "A pseudo-logarithmic framework for edge detection," in *Advances in Computer Vision*, ser. Lecture Notes in Computer Science, J. B.-T. et al, Ed. Springer Verlag, 2008, vol. 5259, pp. 637 – 644.

[6] P. Gremillet, M. Jourlin, and J. Pinoli, "Lip model-based three-dimensional reconstruction and visualisation of hiv infected entire cells," *Journal of Microscopy*, vol. 174, pp. 31–38, 1994.

[7] G. Deng, L. Cahill, and G. Tobin, "The study of logarithmic image processing model and its application to image enhancement," *IEEE Transactions on Image Processing*, vol. 4, no. 4, pp. 506–512, 1995.

[8] A. Oprea, C. Vertan, **C. Florea**, and L. Florea, "A logarithmic-like image processing framework for biomedical image enhancement," *Buletinul Ştiinţific al Universităţii Politehnica din Timişoara*, vol. 53(67), no. 1-2, pp. 66–69, 2008.

[9] **C. Florea**, C. Vertan, and L. Florea, "Logarithmic model-based dynamic range enhancement of hip x-ray images," in *Advances in Computer Vision*, ser. Lecture

Notes in Computer Science, J. B.-T. et al, Ed. Springer Verlag, 2007, vol. 4678, pp. 587–596.

[10] **C. Florea**, C. Vertan, L. Florea, and A. Oprea, "On the use of logarithmic image processing models in total hip prostheses x-ray visualization and analysis," in *Proceedings of the Medical Image Understanding and Analysis, MIUA*, Dundee, United Kingdom, July 2008, pp. 127–131.

[11] V. Pătraşcu and I. Voicu, "An algebraical model for gray level images," in *Proceedings of the Exhibition on Optimization of Electrical and Electronic Equipment, OPTIM*, Braşov, România, 2000, pp. 809–812.

[12] M. Jourlin and J. C. Pinoli, "Logarithmic image processing. the mathematical and physical framework for the representation and processing of transmitted images," *Advances in Imaging and Electron Physics*, vol. 115, no. 1, pp. 129–196, 2001.

[13] V. Pătraşcu, V. Buzuloiu, and C. Vertan, "Fuzzy image enhancement in the framework of logarithmic model," in *Fuzzy Filters for Image Processing*, ser. Studies in Fuzziness and Soft Computing, M. Nachtegael and E. Kerre, Eds. Springer Verlag, March 2003, vol. 122, ch. 10, pp. 219–237.

[14] **C. Florea** and C. Vertan, "Piecewise linear approximation of logaritmic image processing models for dynamic range enhancement," *Buletinul Stiintific al Universitatii Politehnica Bucuresti*, 2009, to be published.

[15] J. Hefferon, *Linear Algebra*. web edition, 2008, http://joshua.smcvt.edu /math/hefferon.html.

[16] B. E. Bayer, "Color imaging array," *U.S. Patent*, no. 3,971,065, 1976.

[17] Y. C. Chang and J. F. Reid, "Rgb calibration for color image analysis in machine vision," *IEEE Transactions on Image Processing*, vol. 5, no. 10, pp. 1414–1422, 1996.

[18] P. Debevec and J. Malik, "Recovering high dynamic range radiance maps from photographs," in *ACM SIGGRAPH Proceedings of the 24th Annual Conference on Computer Graphics and Interactive Techniques*, Los Angeles, California, SUA, August 1997, pp. 369–378.

[19] M. D. Grossberg and S. K. Nayar, "High dynamic range from multiple images: Which exposures to combine?" in *Proceedings of IEEE Workshop on Color and Photometric Methods in Computer Vision at ICCV 2003*, Nice, France, October 2003.

[20] S. Mann and R. Picard, "Being "undigital" with digital cameras: Extending dynamic range by combining differently exposed pictures," in *Proceedings of IS&Ts 48th Annual Conference*, vol. 1, Washington D.C., U.S, May 1995, pp. 422–428.

[21] T. Mitsunaga and S. K. Nayar, "Radiometric self calibration," in *Proceedings of Computer Vision and Pattern Recognition*, vol. 1, Ft. Collins, U.S., June 1999, pp. 374–380.

[22] M. Aguilar and W. Stiles, "Saturation of the rod mechanism of the retina at high levels of stimulation," *Optica Acta*, vol. 1, no. 11, pp. 59–65, 1954.

[23] J. Pinoli, "The logarithmic image processing model: Connections with human brightness perception and contrast estimators," Octomber.

[24] **C. Florea**, F. Albu, C. Vertan, and A. Drîmbărean, "Logarithmic tools for in-camera image processing," in *Proceedings of 16th IET Irish Signals and Systems Conference*, Galway, Irlanda, 2008.

[25] **C. Florea**, C. Vertan, and L. Florea, "Hip prostheses X-ray image processing by LIP exposure prediction," in *Proceedings of Communications 2008*, vol. 1. Bucureşti, România: IEEE, 2008, pp. 121–124.

[26] F. Xiao, J. Pincenti, G. John, and K. Johnson, "Camera motion and mobile imaging," in *Proceedings of the SPIE-IST Electronic-Imaging*, vol. 6502, 2007.

[27] **C. Florea**, F. Albu, A. Zamfir, and A. Drîmbărean, "Handheld article with movement discrimination," *U.S. Patent*, no. 20080231713, 2007.

[28] D. Sachs, S. Nasiri, and D. Goehl, "Image stabilization technology overview," ca. 2005, www.invensense.com.

[29] P. Corcoran, E. Steinberg, P. Bigioi, A. Drîmbaţrean, A. Zamfir, and **C. Florea**, "Image acquisition method and apparatus," *U.S. Patent*, no. US 20070296833, May, 2007.

[30] R. C. Puetter, T. R. Gosnell, and A. Yahil, "Digital image reconstruction:. deblurring and denoising," *Annual Review of Astronomy and Astrophysics*, vol. 43, pp. 139–194, 2005.

[31] F. Xiao, J. Pincenti, and J. Farrell, "Camera motion and effective spatial resolution," in *Proceedings of International Congress of Imaging Science*, vol. 1, May, 2007, pp. 33–36.

[32] S. Perstel, E. Pozniansky, and O. Meitav, "Camera optimization techniques that take camera and scene motion into account," *U.S. Patent*, no. 2007092244, 2007.

[33] N. Sorek and I. Vitsundel, "Enhancing digital photography," *U.S. Patent*, no. 2,006,017,837, January, 2006.

[34] F. Albu, E. Steinberg, A. Drîmbărean, **C. Florea**, A. Zamfir, P. Corcoran, and V. Poenaru, "Image processing method and apparatus," *U.S. Patent*, no. 20080219581, Septembrie, 2007.

[35] G. H. Golub and C. F. V. Loan, *Matrix Computations*. Baltimore, U.S: John Hopkins University Press, 1996, 3rd edition.

[36] H. R. Blackwell, "Contrast thresholds of the human eye," *Journal of the Optical Society of America*, vol. 36, no. 11, pp. 624–643, November 1946.

[37] T. Yamada, K. Ikeda, Y. Kim, H. Wakoh, T. Toma, T. Sakamoto, K. Ogawa, E. Okamoto, K. Masukane, K. Oda, and M. Inuiya, "A progressive scan ccd image sensor for dsc applications," *IEEE Journal of Solid-State Circuits*, vol. 35, no. 12, pp. 2044–2054, December 2000.

[38] S. Nayar and V. Branzoi, "Adaptive dynamic range imaging: Optical control of pixel exposures over space and time," in *IEEE International Conference on Computer Vision (ICCV)*, vol. 2, Nice, France, Octomber 2003, pp. 1168–1175.

[39] Y. Y. Schechner and S. K. Nayar, "Generalized mosaicing: High dynamic range in a wide field of view," *International Journal on Computer Vision*, vol. 53, no. 3, pp. 245–267, July-August 2003.

[40] L. Sirbu, J. Thijssen, **C. Florea**, V. Buzuloiu, and C. deKorte, "Automatic segmentation of the heart muscle from echocardiographic images," in *Proceedings of*

the Internation Symposium on Signals, Circuits and Systems, ISSCS, Iaşi, România, July 2005, pp. 39–42.

[41] K. Sauer and B. Schwartz, "Efficient block motion estimation using integral projections," *IEEE Transaction on Circuits, Systems for Video Tech*, vol. 6, no. 5, pp. 513–518, Octomber 1996.

[42] F. Albu, **C. Florea**, A. Zamfir, and A. Drimbarean, "Low complexity global motion estimation techniques for image stabilization," in *Proceedings of the International Conference on Consumer Electronics, ISSCS*, Las Vegas, U.S., January 2008, pp. 465–467.

[43] C. D. Kuglin and D. C. Hines, "The phase correlation image alignment method," in *Proceedings of the IEEE Conference on Cybernetics and Society*, Bucureşti, România, September 1975, pp. 163–165.

[44] A. Averbuch and Y. Keller, "FFT based image registration," in *Proceedings of IEEE International Conference on Acoustics, Speech and Signal Processing, ICASSP*, vol. 4, Orlando, Florida, U.S., May 2002, pp. 3608–3611.

[45] S. K. Nayar and T. Mitsunaga, "High dynamic range imaging: Spatially varying pixel exposures," in *Proceedings of IEEE Conference on Computer Vision and Pattern Recognition CVPR*, vol. 1, Hilton Head, U.S, June 2000, pp. 472–479.

[46] L. Florea, C. Vertan, **C.. Florea**, and A. Oprea, "Dynamic range enhancement of consumer digital camera acquired hip prosthesis xray images," in *Proceedings of MEDINF*, Sibiu, România, August 2007, pp. 25–26.

[47] D. Colţuc and P. Bolon, "Strict ordering on discrete images and applications," in *Procceedins of IEEE International Conference on Image Processing, ICIP*, vol. 3, Tokio, Japan, 1999, pp. 150 – 153.

[48] L. Florea, C. Vertan, **C. Florea**, and A. Oprea, "Digital acquisition and remote investigation of film radiographies of total hip prostheses," in *Proceedings of EUSIPCO 2007*, Poznan, Polonia, September 2007, pp. 1103–1106.

[49] **C. Florea** and C. Vertan, "Dynamic range enhancement in digital camera acquisition of prostheses hip Xrays," in *Proceedings of International SYmposium on Signals Circuits and Systems, ISSCS*, vol. 1. Iaşi, România: IEEE, 2007, pp. 1–4.

[50] L. Florea, C. Vertan, and **C. Florea**, "Automatic fit estimation of the femoral component of a hip prosthses in digitized radiographies," in *Proceedings of Communications 2008*, vol. 1. Bucureşti, România: IEEE, 2008, pp. 121–124.

[51] C. Vertan, L. Florea, **C.. Florea**, A. Oprea, M. Popescu, and S. Cristea, "Studiul corelaţiei clinico-radiologice al potrivirii componentei femurale a unei proteze totale de şold pe baza monitorizării cu un sistem automat de prelucrare digitală a filmelor radiologice," in *Simpoziomul Naţional pentru Excelenţa în Cercetare Ştiinţifică Medicală*, Sibiu, România, 2008, p. 58.

[52] L. Florea, C. Vertan, and **C.. Florea**, "3D femoral bone approximation in prosthesed hip radiographies," in *Proceedings of 2008 IEEE International Conference on Intelligent Computer Communication and Processing ICCP*, Cluj-Napoca, România, August 2008, pp. 75–82.

[53] C. Vertan, L. Florea, **C. Florea**, A. Oprea, M. Popescu, and S. Cristea, "Clinical-radiological correlation of the fit of the femoral component of a hip prosthesis: Tha follow-up by digital x-ray image processing," in *Proceedings of the Medical Congress EFORT*, Nice, France, May 2008.